CHEMISTRY

Single cycloparaphenylene molecule devices: Achieving large conductance modulation via tuning radial π-conjugation

Yaxin Lv[1,2]†, Junfeng Lin[1,3]†, Kai Song[1], Xuwei Song[1,3], Hongjun Zang[2]*, Yaping Zang[1,3]*, Daoben Zhu[1]*

Conjugated macrocycles cycloparaphenylenes (CPPs) have unusual size-dependent electronic properties because of their unique radially π-conjugated structures. Contrary to linearly π-conjugated molecules, their highest occupied molecular orbital (HOMO)–lowest unoccupied molecular orbital (LUMO) gap shrinks as the molecular size reduces, and this feature can, in principle, be leveraged to achieve unexpected size-dependent transport properties. Here, we examine charge transport characteristics of [n]CPPs (n = 5 to 12) at the single molecule level using the scanning tunneling microscope–break junction technique. We find that the [n]CPPs have a much higher conductance than their linear oligoparaphenylene counterparts at small ring size and at the same time show a large tunneling attenuation coefficient comparable to saturated alkane series. These results show that the radially π-conjugated molecular systems can offer much larger conductance modulation range than standard linear molecules and can be a new platform for building molecular devices with highly tunable transport behaviors.

INTRODUCTION

Hoop-shaped, conjugated macrocycles with radially oriented p-orbitals have gained tremendous recent research interest. The unique radial π-electron delocalization feature renders them unusual properties that are difficult to obtain in linearly π-conjugated systems. As the basic fragments of armchair carbon nanotubes (CNTs) (*1*) and fullerenes (Fig. 1) (*2*), cycloparaphenylenes (CPPs) are one of the most attractive systems among such macrocycles. Since first synthesized in 2008 (*3*), a wealth of unusual properties of CPPs associated with their unique strained cyclic conjugated structures have been discovered (*4–13*). Because of the radially oriented π-systems, CPPs exhibit very special size-dependent electronic properties. For instance, the HOMO-LUMO energy gap of CPPs shrinks as the number of phenylene units decreases (Fig. 1C) (*8, 11, 14–18*). This trend is opposite to that of the linear oligoparaphenylenes (LPPs) and other linearly conjugated molecules and can be attributed to the increased torsion and bending effects in smaller CPPs (*8*). This characteristic makes CPPs appealing candidates as new electronic materials for achieving unexpected charge transport properties. Theoretical studies of the conducting properties of [n]CPPs have been performed recently (*19, 20*), demonstrating the potential applications of [n]CPPs in molecular and organic devices. Despite these theoretical predictions, experimental explorations of [n]CPP-based electronic devices are still very limited. The electronic transport characteristic of [n]CPP-based devices and, in particular, how it is different from the more standard linear systems are still unclear.

In this work, we incorporate the radially π-conjugated [n]CPPs (n = 5 to 12) into single-molecule devices and interrogate their size-dependent transport properties using the scanning tunneling microscope–break junction (STM-BJ) technique (Fig. 2A). We find that, without introducing any heteroatoms as anchors, these [n]CPPs can directly bind to gold electrodes because of the orbital coupling between Au and the curved phenylene rings. We further show that the [n]CPP series has very unique size-dependent conductance characteristics: The conductance of [n]CPPs is significantly higher than their linear LPP counterparts for small n; further, they have a large tunneling attenuation coefficient (β) comparable to saturated alkanes. We emphasize that, achieving both high conductance in a relative short length and large β value within one conjugated system is unprecedented (*21–24*). This characteristic suggests CPPs an ideal system for realizing large conductance modulation by tuning molecular size. Density functional theory (DFT)–based calculations further reveal that the unique size dependence of conductance arises precisely from the radially π-conjugated structures of CPPs. Hence, tuning radial π-conjugation provides a new strategy for efficiently modulating charge transport at the molecular level.

RESULTS

All [n]CPP molecules studied in this work are commercially available (purchased from Tokyo Chemical Industry). We first measure their single-molecule conductance in 1,2,4-trichlorobenzene (TCB; 0.1 mM concentration) using the STM-BJ technique (*25, 26*) under ambient conditions and room temperature. During these measurements, an Au STM tip was repeatedly pushed and pulled to form and break the contact with an Au substrate in the molecular solution. After breaking Au point contacts, the molecule can bridge the STM tip and substrate and form single Au-molecule-Au junctions. We continuously record the conductance distributions as a function of the electrode displacements. In the conductance-displacement trace, we typically observe the conductance plateau at the unit conductance quantum ($G_0 = 2e^2/h$) because of the formation of single Au-Au point contact. The plateau occurred below G_0, signifying the formation of single-molecule junctions. The measured molecular
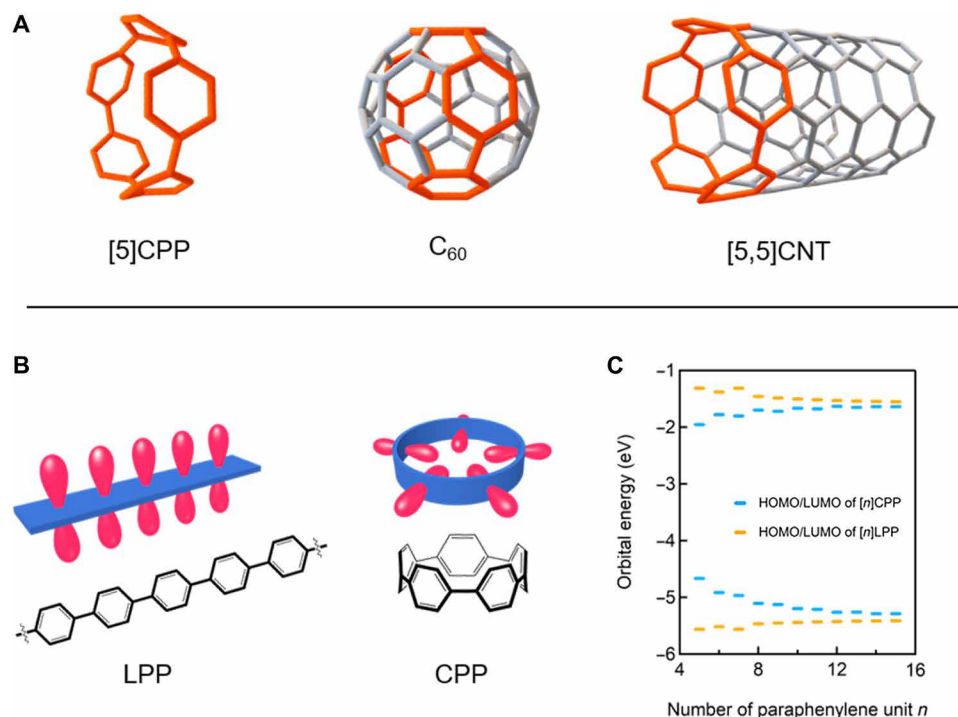
Fig. 1. Structures, orbitals, and orbital energies of CPPs and related molecules. (A) Schematic of [5]CPP, C_{60}, and [5,5]CNT. **(B)** Linear π-conjugation of LPP and radial π-conjugation of CPP. **(C)** Energies of the HOMO and LUMO orbitals in [n]CPP and [n]LPP (n = 5 to 15) (*34*).
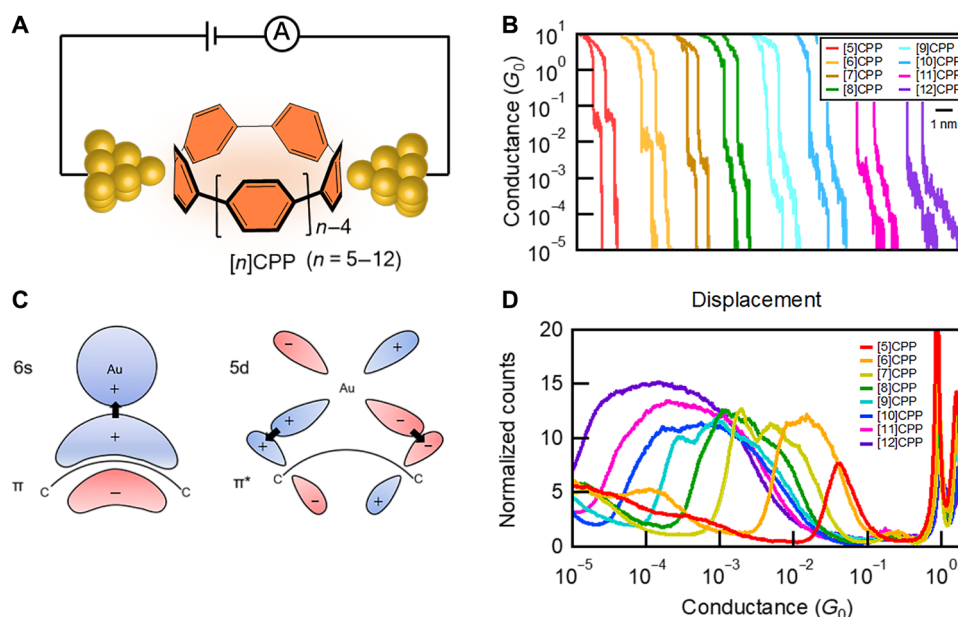

Fig. 2. STM-BJ measurement results of [n]CPPs (n = 5 to 12). (A) Schematic of single-[n]CPP junction. **(B)** Sample conductance traces for [5]CPP-[12]CPP measured under an applied tip bias voltage of 100 mV. **(C)** Schematic of orbital bonding between CPP molecule and Au. **(D)** 1D conductance histograms of [5]CPP-[12]CPP measured under an applied tip bias voltage of 100 mV.

conductance plateau length is related to the length of the formed molecular junctions.

Figure 2B shows sample conductance traces of [5]CPP-[12]CPP measured at an applied tip bias voltage of 100 mV. We see clear molecular conductance plateaus for all these CPP molecules, indicating

the formation of single-[n]CPP junctions. Since no heteroatom anchors are attached in [n]CPPs, we hypothesize that the single-[n]CPP junctions are formed through direct electrode-molecule binding between Au and the distorted phenylene rings. Note that the π-orbitals of the strained [n]CPPs are radially oriented (table S1),

and the interaction between the curved π-orbitals and Au electrodes is strengthened compared with that of conjugated systems composed of flat phenylene units (*27*, *28*). Strain-promoted electrode-molecule binding has also been observed for C_{60} and π-π stacked benzene systems (*29*, *30*) and are attributed to the increased metal affinity of the outer surface of the curved conjugated molecules (*31*, *32*). Analysis of molecular orbital symmetry further indicates that the Au electrodes bind to C—C bonds within the phenylene rings of [*n*]CPPs in η^2-fashion (Fig. 2C). Specifically, the Au-CPP bond is formed because of the electron donation from the filled π-orbital of CPP to the s-orbital of Au, along with the electron back-donation from the filled Au d-orbital to the empty CPP π*-orbital.

We further note from the sample conductance traces that, as the molecular size increases, the conductance of [*n*]CPP series decreases, while the plateau length increases. For larger [*n*]CPPs, the conductance plateau also becomes more sloped. Figure 2D and fig. S1 present the one-dimensional (1D) conductance histograms compiled from thousands of conductance traces of [*n*]CPPs without any data selection. In these histograms, we observe that as *n* increases from 5 to 12, the conductance decreases while the conductance peak becomes more spread. In addition, the corresponding 2D conductance-displacement histograms reveal that the molecular conductance plateaus have longer extensions and wider conductance distributions for larger [*n*]CPPs (see Fig. 3, A and B, and fig. S2). Note that in CPPs, every phenylene unit can, in principle, provide multiple binding sites based on which single-molecule junctions can be formed. For larger CPPs, the increase in the binding sites enables the creation of multiple junction conformations through forming Au-CPP contacts at different pairs of binding sites, resulting in multiple overlapping conductance peaks (or one broad peak). Moreover, as we retract the STM tip away from the substrate, the phenylene binding sites can switch from one pair to another and cause the conductance decrease until the electrode separation reaches the maximum (fig. S3), hence yielding the sloped conductance plateaus shown in the 2D histograms. This switch effect is further rationalized through DFT-based transport calculations (see the Supplementary Materials for detailed discussions).

To gain deeper insight into charge transport properties of [*n*]CPPs, we compare the conductance of junctions formed with different molecules in this series. For each molecule, we fit the conductance peak corresponding to the junction conformation where the distance between the two binding sites reaches the maximum (referred to as transport length). Note that for larger CPPs with multiple conductance peaks, the lowest conductance peak corresponding to the longest junction conformation is fitted (see fig. S4). [11]CPP and [12]CPP are not included as their conductance peaks are too broad. We plot the peak conductance against the transport length for these CPP molecules and observe an exponential length dependence of conductance, indicating a coherent tunneling transport mechanism (fig. S5) (*33*). To include the whole series of [*n*]CPPs, we determine their conductance from a profile taken at the end of molecular conductance plateaus in the 2D histograms (see inset of Fig. 3, A and B, and figs. S2 and S5A). As can be seen from fig. S5B, the conductance obtained from the 1D and 2D histograms are almost identical. By further fitting the data, we obtain the β value, ~7.4/nm, which is much larger than that reported for LPPs (~4/nm). To the best of our knowledge, the β value of the [*n*]CPP series is the largest among that of the conjugated molecular wires reported so far and is comparable to saturated alkanes (8.3/nm) (*34*). It should be further noted that, despite having a larger β value, the [*n*]CPP series show significant higher conductance than amine-terminated LPP series at a relatively short length (<1.8 nm), and the measured [5]CPP-[8]CPP molecules all fall into this region. The contact resistance, which is the *Y*-intercept of the fitted curve, is estimated to be 105.8 ohms for the [*n*]CPP series. Note that this contact resistance is much lower than amine terminated LPPs (47.5 kilohms) and alkanes (19.7 kilohms), and this fact contributes to the higher conductance of CPPs at shorter transport distance. It is also interesting to compare the conductance of CPPs and LPPs using a "through-bond" distance, in which case, the conductance of CPPs is even larger and the β value is smaller (see fig. S6 for more details). Together, the [*n*]CPP series shows both remarkably high conductance in a relative short transport length and large β value, two characteristics which typically do not coexist within one molecular system.

To better understand the unique size-dependent conductance properties, we turn to DFT-based calculations. We first optimize the junctions formed with the [*n*]CPP series using the Fritz Haber Institute ab initio molecular simulation (FHI-AIMS) package with a Perdew-Burke-Ernzerhof (PBE) exchange-correlation functional (see the Supplementary Materials for the detailed calculation methods)
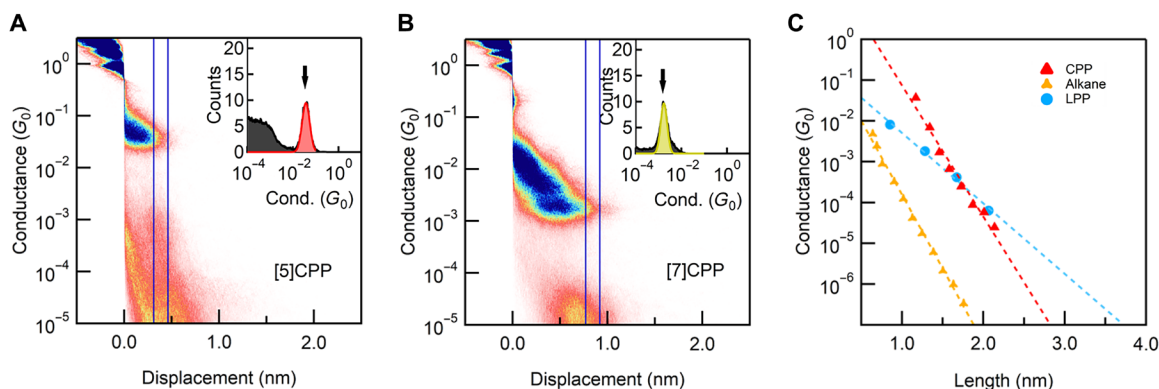

Fig. 3. Length-dependent conductance of [*n*]CPPs. (A and **B)** 2D conductance-displacement histograms of [5]CPP and [7]CPP. The vertical lines at the end of the molecular feature indicate the window (0.15 nm) for determining the conductance profiles shown in the inset. (**C**) Conductance of [5]CPP-[12]CPP determined from the profiles in the 2D histograms against calculated transport length (Au-Au distance). Conductance of amine-terminated LPPs and alkanes (measured in TCB solvent) against length are included for reference (*47*). The β value (obtained via data fitting) is ~7.4/nm for CPPs, ~4.0/nm for LPPs, and 8.3/nm for alkanes.

(*35–41*) and find that the Au electrode binds to the phenylene unite in η^2 fashion (Fig. 4A), similar to the ethylene-Au complex (*42*), and agrees with our analysis of CPP-Au bonding based on molecular orbital symmetry (Fig. 2C). We then calculate the binding energy between the [*n*]CPP molecule and the Au electrode (fig. S7), and find that the binding energy slightly decreases when the molecular size increases. This trend is expected since the decreased ring curvature in the larger CPPs leads to decreased molecule-electrode affinity (*32*, *43*). We next calculate the transmission functions of these optimized geometries and plot the calculated transmissions against energy (Fig. 4B). We note that for this molecular series, the energy separation between HOMO and LUMO resonances decreases as the size of CPPs shrinks, in agreement with the HOMO-LUMO gaps determined by optical and electrochemical characterizations (*10*, *44*). Since the HOMO and LUMO resonances are very sensitive to the computational method, we thus focus on the qualitative trends. Notably, the trend of HOMO-LUMO gap changes is opposite to that of linearly conjugated molecules, of which the gap narrows as the molecule becomes longer because of the extended conjugation (*45*, *46*). In contrast, in radially conjugated [*n*]CPPs, by decreasing the size, the increased ring strain lowers the torsional angles between the phenylene units, thus facilitating the radial π-electron delocalization. In addition, the increased bending of individual phenylene promotes antibonding interactions between orbital lobes on adjacent phenylene units. These effects together increase the radial π-conjugation and narrows the HOMO-LUMO gap in the smaller CPPs (*11*, *15–18*).

Further inspecting on the transmissions reveals that the electrode-molecule coupling strength, which is reflected by the width of resonance, decreases as the size of [*n*]CPPs increases. The decreased coupling, along with the increased energy separation of HOMO and LUMO resonances, leads to an obvious decrease in transmission at E_F from [5]CPP to [10]CPP. Moreover, we obtain the theoretical β value of 7.94/nm by plotting the zero-bias transmission (at E_F) against the transport length (see inset of Fig. 4B and fig. S8). This is in good agreement with the experimental result.

DISCUSSION
In conclusion, we have studied single-molecule conductance of a series of strained [*n*]CPPs (*n* = 5 to 12) with radially oriented
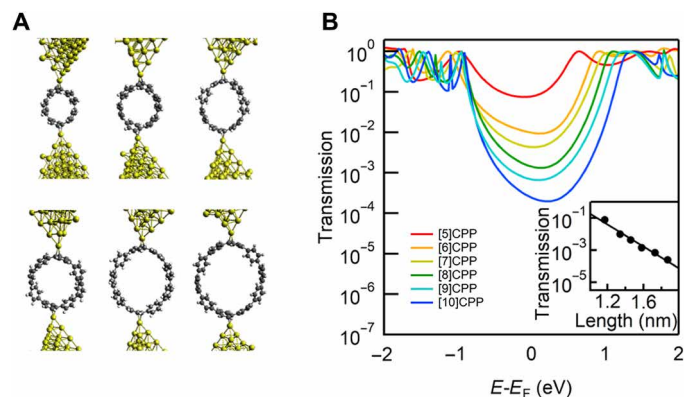
π-orbitals using the STM-BJ technique. We have demonstrated that compared with the LPPs, the CPP series simultaneously shows much higher conductance at a relative short transport length and a larger tunneling attenuation coefficient similar to saturated alkanes. This size-dependent conducting feature indicates the possibility of achieving large conductance modulation range beyond that can be obtained in standard linearly conjugated systems. Through DFT-based calculations, we attribute this feature to the unique structures related to strain and radial π-conjugation presented in CPPs. These results suggest that, beyond the standard linear π-conjugation, radial π-conjugation could be leveraged for achieving large modulation of molecular charge transport properties. We anticipate these results will stimulate future work on designing new functional electronic materials and devices capitalizing on unconventional π-conjugation patterns.

MATERIALS AND METHODS
STM-BJ measurements
All [*n*]CPP (*n* = 5 to 12) molecules were purchased from Tokyo Chemical Industry and directly used without further purification. Single-molecule conductance measurements were carried out using a custom-built STM-BJ platform. All the STM-BJ experiments were performed in ambient conditions and room temperature. Single-molecule conductance measurements were made in [*n*]CPP solutions (0.1 mM concentration), where TCB purchased from Alfa Aesar was used as the solvent. During the conductance measurements, the Au tip and the substrate coated with a gold layer were used as the two electrodes. Under an applied tip bias voltage of 100 mV, the Au tip was driven to move in and out of contact with the substrate deposited with [*n*]CPP solutions to form and break Au-CPP-Au molecule junctions. During this process, the current was recorded continuously, and the conductance was calculated by the formula $G = I/V$. One-dimensional conductance histograms and the 2D conductance histograms were constructed by compiling thousands of collected conductance traces without any data selection.

DFT-based calculations
We attached two Au clusters containing four Au atoms to the two sides of the optimized molecular structure and relax the junction geometries using the PBE exchange-correlation functional implemented by the FHI-AIMS packages (*36*, *37*, *40*). After relaxation, the 4 atom Au clusters were replaced by Au pyramids containing 60 Au atoms in six layers, and the binding energy were calculated using the same basis for both gold and molecule. The Landauer transmission across the junctions were calculated using the non-equilibrium Green's function formalism.

REFERENCES AND NOTES
1. J. Xia, R. Jasti, Synthesis, characterization, and crystal structure of [6]cycloparaphenylene. *Angew. Chem. Int. Ed.* **51**, 2474–2476 (2012).
2. S. Yamago, E. Kayahara, T. Iwamoto, Organoplatinum-mediated synthesis of cyclic π-Conjugated molecules: Towards a new era of three-dimensional aromatic compounds. *Chem. Rec.* **14**, 84–100 (2014).
3. R. Jasti, J. Bhattacharjee, J. B. Neaton, C. R. Bertozzi, Synthesis, characterization, and theory of [9]-, [12]-, and [18]cycloparaphenylene: Carbon nanohoop structures. *J. Am. Chem. Soc.* **130**, 17646–17647 (2008).

Fig. 4. DFT-based transmission calculations of [*n*]CPPs. (A) Single-[*n*]CPP junction geometries (*n* = 5 to 10) used in transmission calculations. **(B)** Calculated transmissions against energy for single-[*n*]CPP junctions. Inset: Transmission at E_F as a function of transport length. The calculated β value is 7.9/nm.

4. E. J. Leonhardt, R. Jasti, Emerging applications of carbon nanohoops. *Nat. Rev. Chem.* **3**, 672–686 (2019).

5. E. Kayahara, V. K. Patel, S. Yamago, Synthesis and characterization of [5]cycloparaphenylene. *J. Am. Chem. Soc.* **136**, 2284–2287 (2014).

6. E. Kayahara, L. Sun, H. Onishi, K. Suzuki, T. Fukushima, A. Sawada, H. Kaji, S. Yamago, Gram-scale syntheses and conductivities of [10]cycloparaphenylene and its tetraalkoxy derivatives. *J. Am. Chem. Soc.* **139**, 18480–18483 (2017).

7. P. J. Evans, E. R. Darzi, R. Jasti, Efficient room-temperature synthesis of a highly strained carbon nanohoop fragment of buckminsterfullerene. *Nat. Chem.* **6**, 404–408 (2014).

8. M. R. Golder, R. Jasti, Syntheses of the smallest carbon nanohoops and the emergence of unique physical phenomena. *Acc. Chem. Res.* **48**, 557–566 (2015).

9. H. Omachi, Y. Segawa, K. Itami, Synthesis of cycloparaphenylenes and related carbon nanorings: A step toward the controlled synthesis of carbon nanotubes. *Acc. Chem. Res.* **45**, 1378–1389 (2012).

10. E. Kayahara, K. Fukayama, T. Nishinaga, S. Yamago, Size dependence of [n]cycloparaphenylenes (n=5–12) in electrochemical oxidation. *Chem. Asian J.* **11**, 1793–1797 (2016).

11. Y. Segawa, A. Fukazawa, S. Matsuura, H. Omachi, S. Yamaguchi, S. Irle, K. Itami, Combined experimental and theoretical studies on the photophysical properties of cycloparaphenylenes. *Org. Biomol. Chem.* **10**, 5979–5984 (2012).

12. F. Lucas, N. McIntosh, E. Jacques, C. Lebreton, B. Heinrich, B. Donnio, O. Jeannin, J. Rault-Berthelot, C. Quinton, J. Cornil, C. Poriel, [4]Cyclo-*N*-alkyl-2,7-carbazoles: Influence of the alkyl chain length on the structural, electronic, and charge transport properties. *J. Am. Chem. Soc.* **143**, 8804–8820 (2021).

13. M. Iyoda, J. Yamakawa, M. J. Rahman, Conjugated macrocycles: Concepts and applications. *Angew. Chem. Int. Ed.* **50**, 10522–10553 (2011).

14. C. Evangeli, K. Gillemot, E. Leary, M. T. González, G. Rubio-Bollinger, C. J. Lambert, N. Agraït, Engineering the thermopower of C$_{60}$ molecular junctions. *Nano Lett.* **13**, 2141–2145 (2013).

15. C. E. Colwell, T. W. Price, T. Stauch, R. Jasti, Strain visualization for strained macrocycles. *Chem. Sci.* **11**, 3923–3930 (2020).

16. M. Peña Alvarez, P. M. Burrezo, M. Kertesz, T. Iwamoto, S. Yamago, J. Xia, R. Jasti, J. T. L. Navarrete, M. Taravillo, V. G. Baonza, J. Casado, Properties of sizeable [n]cycloparaphenylenes as molecular models of single-wall carbon nanotubes elucidated by Raman spectroscopy: Structural and electron-transfer responses under mechanical stress. *Angew. Chem. Int. Ed.* **53**, 7033–7037 (2014).

17. G. M. Peters, G. Grover, R. L. Maust, C. E. Colwell, H. Bates, W. A. Edgell, R. Jasti, M. Kertesz, J. D. Tovar, Linear and radial conjugation in extended π-electron systems. *J. Am. Chem. Soc.* **142**, 2293–2300 (2020).

18. M. R. Talipov, R. Jasti, R. Rathore, A circle has no end: Role of cyclic topology and accompanying structural reorganization on the hole distribution in cyclic and linear poly-p-phenylene molecular wires. *J. Am. Chem. Soc.* **137**, 14999–15006 (2015).

19. J. B. Lin, E. R. Darzi, R. Jasti, I. Yavuz, K. N. Houk, Solid-state order and charge mobility in [5]- to [12]cycloparaphenylenes. *J. Am. Chem. Soc.* **141**, 952–960 (2019).

20. L. Hu, Y. Guo, X. Yan, H. Zeng, J. Zhou, Electronic transport properties in [n]cycloparaphenylenes molecular devices. *Phys. Lett. A* **381**, 2107–2111 (2017).

21. S. H. Choi, B. Kim, C. D. Frisbie, Electrical resistance of long conjugated molecular wires. *Science* **320**, 1482–1486 (2008).

22. R. M. Metzger, Unimolecular electronics. *Chem. Rev.* **115**, 5056–5115 (2015).

23. T. A. Su, M. Neupane, M. L. Steigerwald, L. Venkataraman, C. Nuckolls, Chemical principles of single-molecule electronics. *Nat. Rev. Mater.* **1**, 16002 (2016).

24. P. Moreno-García, M. Gulcur, D. Z. Manrique, T. Pope, W. Hong, V. Kaliginedi, C. Huang, A. S. Batsanov, M. R. Bryce, C. Lambert, T. Wandlowski, Single-molecule conductance of functionalized oligoynes: Length dependence and junction evolution. *J. Am. Chem. Soc.* **135**, 12228–12240 (2013).

25. B. Xu, N. J. Tao, Measurement of single-molecule resistance by repeated formation of molecular junctions. *Science* **301**, 1221–1223 (2003).

26. L. Venkataraman, J. E. Klare, C. Nuckolls, M. S. Hybertsen, M. L. Steigerwald, Dependence of single-molecule junction conductance on molecular conformation. *Nature* **442**, 904–907 (2006).

27. T. Yelin, R. Korytár, N. Sukenik, R. Vardimon, B. Kumar, C. Nuckolls, F. Evers, O. Tal, Conductance saturation in a series of highly transmitting molecular junctions. *Nat. Mater.* **15**, 444–449 (2016).

28. J. S. Meisner, S. Ahn, S. V. Aradhya, M. Krikorian, R. Parameswaran, M. Steigerwald, L. Venkataraman, C. Nuckolls, Importance of direct metal–π coupling in electronic transport through conjugated single-molecule junctions. *J. Am. Chem. Soc.* **134**, 20440–20445 (2012).

29. C. A. Martin, D. Ding, J. K. Sørensen, T. Bjørnholm, J. M. van Ruitenbeek, H. S. J. van der Zant, Fullerene-based anchoring groups for molecular electronics. *J. Am. Chem. Soc.* **130**, 13198–13199 (2008).

30. S. T. Schneebeli, M. Kamenetska, Z. Cheng, R. Skouta, R. A. Friesner, L. Venkataraman, R. Breslow, Single-molecule conductance through multiple π–π-stacked benzene rings determined with direct electrode-to-benzene ring connections. *J. Am. Chem. Soc.* **133**, 2136–2139 (2011).

31. W. Kicinski, S. Dyjak, Transition metal impurities in carbon-based materials: Pitfalls, artifacts and deleterious effects. *Carbon* **168**, 748–845 (2020).

32. A. Hirsch, Principles of fullerene reactivity, in *Topics in Current Chemistry* (Springer, New York, ed. 1, 1999), pp.5.

33. A. Nitzan, Electron transmission through molecules and molecular interfaces. *Annu. Rev. Phys. Chem.* **52**, 681–750 (2001).

34. Y. Zang, A. Pinkard, Z. F. Liu, J. B. Neaton, M. L. Steigerwald, X. Roy, L. Venkataraman, Electronically transparent Au–N bonds for molecular junctions. *J. Am. Chem. Soc.* **139**, 14845–14848 (2017).

35. A. Bagrets, Spin-polarized electron transport across metal-organic molecules: A density functional theory approach. *J. Chem. Theory. Comput.* **9**, 2801–2815 (2013).

36. V. Havu, V. Blum, P. Havu, M. Scheffler, Efficient integration for all-electron electronic structure calculation using numeric basis functions. *J. Comput. Phys.* **228**, 8367–8379 (2009).

37. V. Blum, R. Gehrke, F. Hanke, P. Havu, V. Havu, X. Ren, K. Reuter, M. Scheffler, Ab initio molecular simulations with numeric atom-centered orbitals. *Comput. Phys. Commun.* **180**, 2175–2196 (2009).

38. A. Arnold, F. Weigend, F. Evers, Quantum chemistry calculations for molecules coupled to reservoirs: Formalism, implementation, and application to benzenedithiol. *J. Chem. Phys.* **126**, 174101 (2007).

39. J. E. M. Soler, E. Artacho, J. D. Gale, A. García, J. Junquera, P. Ordejón, D. Sánchez-Portal, The SIESTA method for ab initio order-N materials simulation. *J. Phys. Condens. Matter* **14**, 2745–2779 (2002).

40. J. P. Perdew, K. Burke, M. Ernzerhof, Generalized gradient approximation made simple. *Phys. Rev. Lett.* **77**, 3865–3868 (1996).

41. P. Ordejón, E. Artacho, J. M. Soler, Self-consistent order-*N* density-functional calculations for very large systems. *Phys. Rev. B* **53**, R10441–R10444 (1995).

42. B. W. Hoogenboom, R. Hesper, L. H. Tjeng, G. A. Sawatzky, Charge transfer and doping-dependent hybridization of C$_{60}$ on noble metals. *Phys. Rev. B* **57**, 11939–11942 (1998).

43. A. Hirsch, Functionalization of single-walled carbon nanotubes. *Angew. Chem. Int. Ed.* **41**, 1853–1859 (2002).

44. T. Nishihara, Y. Segawa, K. Itami, Y. Kanemitsu, Excited states in cycloparaphenylenes: Dependence of optical properties on ring length. *J. Phys. Chem. Lett.* **3**, 3125–3128 (2012).

45. T. Iwamoto, Y. Watanabe, Y. Sakamoto, T. Suzuki, S. Yamago, Selective and random syntheses of [n]cycloparaphenylenes (n=8-13) and size dependence of their electronic properties. *J. Am. Chem. Soc.* **133**, 8354–8361 (2011).

46. Y. Zang, S. Ray, E. D. Fung, A. Borges, M. H. Garner, M. L. Steigerwald, G. C. Solomon, S. Patil, L. Venkataraman, Resonant transport in single diketopyrrolopyrrole junctions. *J. Am. Chem. Soc.* **140**, 13167–13170 (2018).

47. M. S. Hybertsen, L. Venkataraman, J. E. Klare, A. C. Whalley, M. L. Steigerwald, C. Nuckolls, Amine-linked single-molecule circuits: Systematic trends across molecular families. *J. Phys. Condens. Matter* **20**, 374115 (2008).